# Detector performance of the space-borne Doppler wind lidar aboard the Aeolus satellite


Oliver Lux[1], Robert Reichert[1], Christian Lemmerz[1], Nafiseh Masoumzadeh[2], Denny Wernham[3], Trismono Candra Krisna[3], Denis Marchais[4], Ray Bell[5], Tommaso Parrinello[6], Oliver Reitebuch[1]

*[1]Deutsches Zentrum für Luft- und Raumfahrt, Institut für Physik der Atmosphäre, Oberpfaffenhofen, Germany; [2]Max Planck Institute for Extraterrestrial Physics, Garching, Germany; [3]European Space Agency – ESTEC, Noordwijk, The Netherlands; [4]Airbus Defence and Space, Toulouse, France; [5]Teledyne e2v, Chelmsford, United Kingdom; [6]European Space Agency – ESRIN, Frascati, Italy*


## Design and operation principle of the ALADIN detectors

- Doppler frequency shift of cloud/aerosol and molecular backscatter is derived from **two complementary receiver channels** (Mie and Rayleigh), each employing an accumulation charge-coupled device (ACCD).
- ACCDs from Teledyne e2v offer **high quantum efficiency** in the UV (85%) and **low readout noise**.
- Signals from receiver spectrometers were recorded on illuminated **image zones** with 16 x 16 pixels and integrated over time with 25 vertical range gates from 2.1 µs to 16.8 µs (250 m to 2000 m resolution).
- Signals from a settable number of laser pulses are accumulated in the **memory zone** for each range gate, before the charges are read out at 48 kHz and digitized in a detection electronics unit.

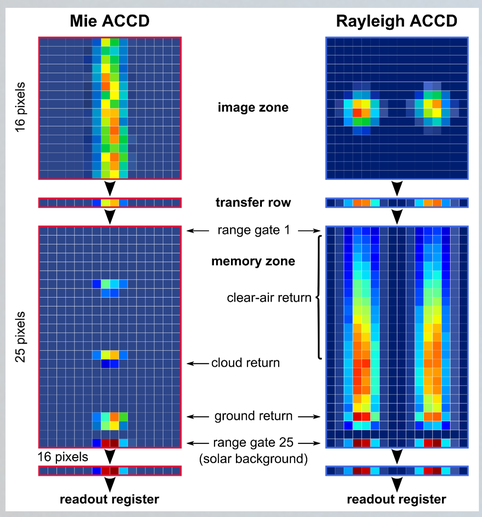


| Specification | Value |
|---|---|
| Type | Thinned backside-illuminated accumulation Si-CCD |
| Area | Image zone: 0.43 mm × 0.43 mm – 16 × 16 pixels<br>Memory zone: 0.43 mm × 0.75 mm – 32 × 25 pixels |
| Pixel size | Image zone: 27 µm × 27 µm<br>Memory zone: 30 µm × 13.5 µm |
| Temporal resolution | 2.1 to 16.8 µs / 250 to 2000 m for atmospheric range gates (#1 to #24); 625 µs / 1250 µs / 3750 µs for solar background (range gate #25) |
| Quantum efficiency | 0.85 |
| Charge-transfer efficiency | 0.999 |
| Radiometric gain | Mie: 0.684 LSB/$e^-$; Rayleigh: 0.434 LSB/$e^-$ |
| Operating temperature | -30 °C |
| Dark current signal rate (rms) | Mie: (0.72 ± 0.31) $e^-s^{-1}$; Rayleigh: (0.64 ± 0.31) $e^-s^{-1}$ (measured in orbit) |
| Dark current signal noise (rms) | 0.78 to 0.89 $e^-$ (measured in orbit) |
| Readout noise (rms) | (5.6 ± 0.2) $e^-$ (measured in orbit) |

*Left: Schematic diagram of the ALADIN ACCD design with exemplary signals measured in the image zone and transferred to the memory zone of the Mie and Rayleigh channel detectors. Right: Specifications and important parameters of the ALADIN ACCDs measured on-ground and in-orbit.*

## Hot pixels and correction scheme

- **Dark current anomalies** appeared on individual pixels of both ACCD memory zones, referred to as **hot pixels**, introducing large systematic errors of the Aeolus wind and aerosol data products.
- Hot pixels resulted from **displacement damages** in the semiconductor lattice caused by high-energy particles like protons, leading to **increased dark current rates** and **random telegraph signals (RTS)**.
- **Increasing number of hot pixels** over the course of the mission lifetime almost linearly with successive hot pixel onsets occurring every ~23 days on average, but long gaps in autumn 2021 and autumn 2022.
- Hot pixels **predominantly activated around the poles** and the **South Atlantic Anomaly** region, where the weakened magnetic field at 320 km Aeolus satellite orbit altitude increased cosmic radiation exposure.
- **Regular dark current calibration**, named "Down Under Dark Experiment" (DUDE), was established in 2019 to **measure dark currents without lidar contributions** and carried out up to eight times per day.
- **Implementation of DUDE procedure largely eliminated systematic errors** which ensured positive impact of Aeolus wind observations on numerical weather prediction forecasts.

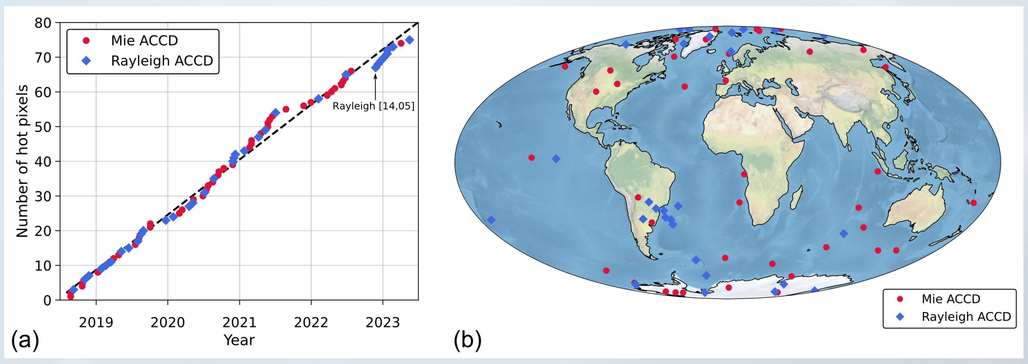


*(a) Temporal progression of the number of hot pixels throughout the mission timeline. (b) Geolocation of the satellite during the activation of individual hot pixels (only if data for the exact activation time is available). Mie and Rayleigh hot pixels are represented by red dots and blue diamonds, respectively.*

## Dark current behavior and hot pixel classification

- Data from **8500 DUDE measurements covering the Aeolus mission** were analyzed to study the temporal evolution of dark current levels on hot pixels.
- **Segmentation approach** based on python ruptures package identified shifts in dark current and **resolved discrete levels** for hot pixels with RTS behavior.
- Statistical analysis allowed for a **classification of the 75 hot pixels** according to their dark current characteristics.
- **Most hot pixels show RTS features**, others display rare shifts or slow drifts in the elevated dark current levels; also combination of both effects occurred.

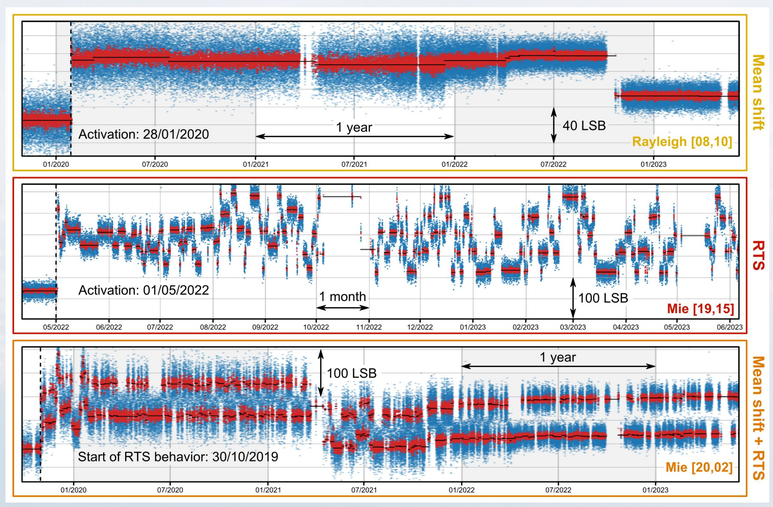


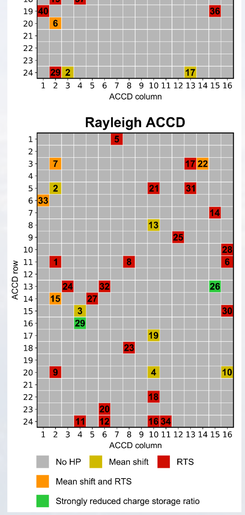


*Left: Time series of the dark current levels for three selected hot pixels with different temporal noise characteristics. Right: Map of hot pixels on the Mie (top) and Rayleigh ACCD (bottom) indicating the temporal dark current behavior and the chronological order of the activation on the respective detector.*

## Hot pixel statistics

- Analysis of segmented dark current time series yielded **statistical parameters of RTS transitions**.
- **Amplitude of RTS transitions range from a few to hundreds of least significant bits (LSB)** (1 LSB ≈ 1.46 electrons for Mie channel ACCD, 2.30 electrons for Rayleigh channel ACCD).
- **Typical lifetimes of RTS levels are of the order of tens of hours to a few days**.
- **Shorter lifetimes (higher transition rates) tend to go along with larger step sizes**.
- The **highest transition rates** (>5 transitions per week) and **largest amplitudes** (>100 LSB) were **mostly found for hot pixels on the Mie channel ACCD**.
- Statistical parameters help **distinguish real RTS transitions from atmospheric signal variations**, which is crucial for the reprocessing of Aeolus data products during mission phase F (2024 – 2028).
- Distinction is **important for detecting RTS steps** and **creating dark current correction files**, especially during periods with few or no DUDE measurements at the beginning of the mission.

| Parameter | Mie ACCD | Rayleigh ACCD |
|---|---|---|
| Hot pixels with shifts in the mean dark current | 12 | 6 |
| Hot pixels with RTS behavior | 24 | 24 (2 showed additional charge storage anomaly) |
| Hot pixels with combination of mean shifts and RTS behavior | 5 | 4 |
| **Total number of hot pixels** (percentage of all ACCD pixels) | **41** (10.7%) | **34** (8.9%) |

*Overview of different classes of hot pixels on the Mie and Rayleigh ACCD in terms of the temporal behavior of the dark current levels.*

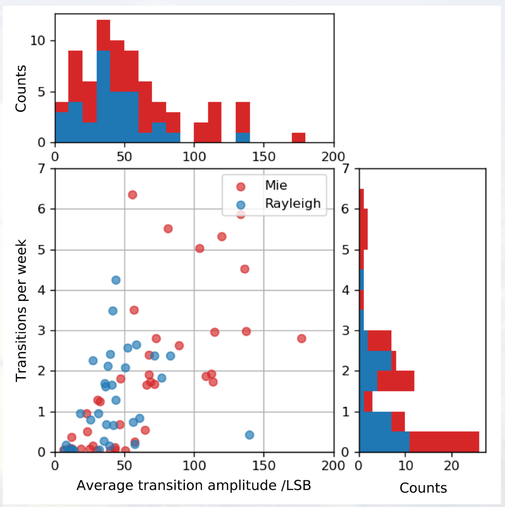


*Correlation between transition rate and transition amplitude derived from the statistical analysis of all hot pixels showing multiple dark current levels.*

## Temperature dependence of the dark current rate

- **Special in-orbit tests** were conducted after the Aeolus mission concluded in April 2023 to **gain insights into the instrument** and **prepare for future space lidar missions like EarthCARE and Aeolus-2**.
- Tests included examining the **temperature dependence of dark current rates**, especially in hot pixels.
- ACCD **temperature was increased from -30 °C to -15 °C in 5 °C increments**, with each non-nominal temperature maintained for 4.5 hours to determine dark current rates for each memory zone pixel.
- Temperature dependence follows the **Arrhenius law**:

$$\mathrm{DC}(T) = \mathrm{DC}_0 \exp(-E_a / k_\mathrm{B} T).$$

DC: Dark current rate
$\mathrm{DC}_0$: Dark current rate at $T = 0$ K
$E_a$: Activation energy
$k_\mathrm{B}$: Boltzmann constant
$T$: Absolute temperature

- **Activation energy can be derived from** the slope of a linear fit in the **Arrhenius plot**.
- **RTS transitions** occurring during the temperature test **may affect** median values and thus **fit results**.

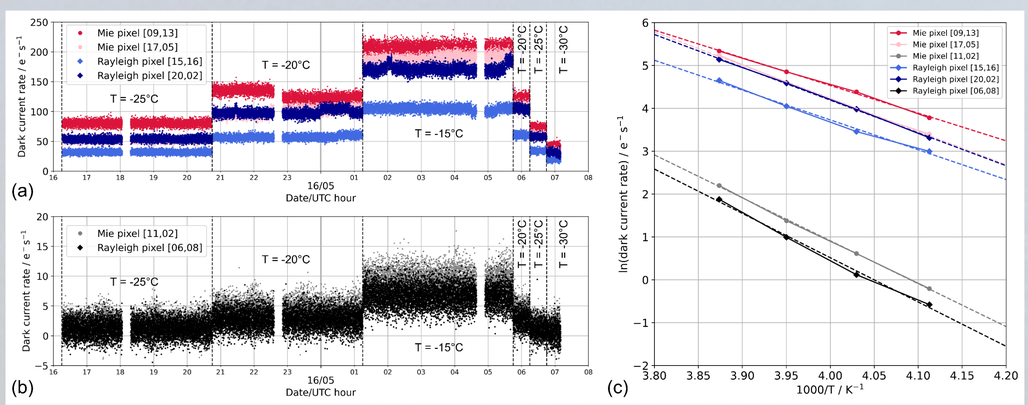


*The time series of the Mie and Rayleigh dark current rates during the ACCD temperature test in May 2023 for selected (a) hot pixels and (b) normal pixels. The median values for each pixel are plotted in the Arrhenius plot (c) from which the activation energy can be determined as the slope of a linear fit.*

## Activation energy and correlation with dark current rate

- **Activation energies are consistent across both ACCDs** (median ≈ 0.87 eV for normal pixels).
- Values are **~25% lower for hot pixels**, supporting the hypothesis that anomalies **are dominated by radiation-induced displacement damages** (clock-induced charges show weak $T$-dependency).
- At nominal ACCD temperature (-30 °C), **dark current rates for normal pixels were (0.7±0.3) $e^-s^{-1}$**.
- **Hot pixel dark current rates** range from a few to several **tens of electrons per second**, up to 90 $e^-s^{-1}$.
- **Extrapolated dark current rates of normal pixels at -50 °C (foreseen for Aeolus-2) are ~40x lower**.
  → **2/3 of hot pixels would have dark current rates comparable to normal pixels at -30 °C**.
- **Activation energy decreases with dark current rate for normal pixels**, while hot pixels show a more scattered pattern suggesting field-enhanced emission in the bulk defects caused by proton irradiation.

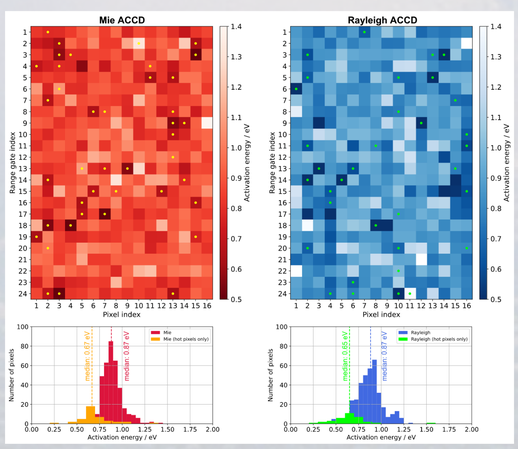


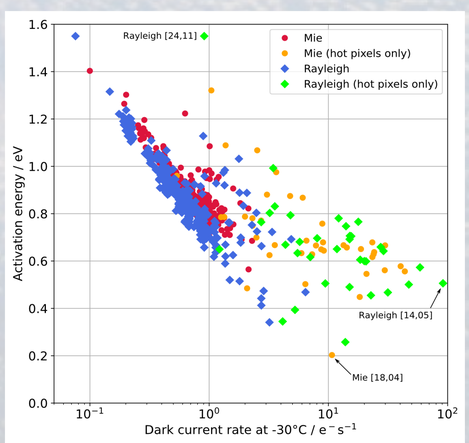


*Left: Activation energy of individual pixels on the Mie and Rayleigh ACCD memory zones. Hot pixels are indicated by dots. The corresponding histograms are shown in the bottom panels. Right: Activation energy versus dark current rate for all pixels of the Mie (circles) and Rayleigh ACCD (diamonds).*


**Deutsches Zentrum für Luft- und Raumfahrt**

**Institut für Physik der Atmosphäre**

http://www.dlr.de/en/pa



O. Lux, R. Reichert, C. Lemmerz, N. Masoumzadeh, D. Wernham, T. C. Krisna, D. Marchais, R. Bell, T. Parrinello, and O. Reitebuch, "CCD detector performance of the space-borne Doppler wind lidar ALADIN during the Aeolus mission," Appl. Opt. 63, 6754-6775 (2024).